Solar Energy Materials and Solar Cells 169 (2017) 56–60

Contents lists available at ScienceDirect

Solar Energy Materials and Solar Cells

journal homepage: www.elsevier.com/locate/solmat

Interpretation of photovoltaic performance of *n*-ZnO:Al/ZnS:Cr/p-GaP solar cell

Mohammadreza Nematollahi[a,*], Esther López[b], Iñigo Ramiro[b], Pablo G. Linares[b], Elisa Antolín[b], Irene Artacho[b], César Tablero[b], Eric Karhu[a], Turid W. Reenaas[a], Antonio Martí[b]

[a] Department of Physics, Norwegian University of Science and Technology, 7491 Trondheim, Norway
[b] Instituto de Energía Solar, Universidad Politécnica de Madrid ETSI Telecomunicación, Ciudad Universitaria s/n, 28040 Madrid, Spain

ARTICLE INFO

Keywords:
Deep-level intermediate band solar cell
Transition-metal-doped semiconductor
Cr-doped ZnS
Thermal carrier escape

ABSTRACT

We investigate Cr-doped ZnS (ZnS: Cr) as a potential deep-level intermediate band material for high efficiency solar cells. We study *n*-ZnO:Al/ZnS:Cr/p-GaP heterojunction cell for the first time, and this paper presents an interpretation of the performance of the solar cell in the framework of intermediate band solar cells. We conclude that the ZnS:Cr used in this work has two characteristic energy levels at 0.88 eV and 2.68 eV below the conduction band. This material also has a quasi-continuum of energy levels between the former level and the valence band maximum. This quasi-continuum results in thermal carrier escape that limits the open-circuit voltage to the lowest energy gap in ZnS: Cr, ≃0.8 V.

1. Introduction

In intermediate band (IB) materials, at least one additional energy level is present in the semiconductor energy gap, allowing the material to absorb sub-bandgap photons. When IB materials are used in intermediate band solar cells (IBSCs), the photo-generated current increases. As long as the charge carriers are extracted from the conduction band (CB) and the valence band (VB) only, a high voltage over the IBSC can be maintained. Thus, IBSCs can potentially be highly efficient solar cells [1]. Reviews of the operation of IBSCs and the progress in the research can be found in Refs. [2,3]. Three types of IB materials have been investigated for the realization of IBSCs, namely, materials based on (i) quantum dots [4], (ii) highly mismatched alloys [5], and (iii) deep-levels (DLs) [6]. So far, none of the IB materials investigated have resulted in high-efficiency IB solar cells. Progress towards the production of such high-efficiency cells requires development of new IB materials.

The two operating principles of an IBSC are *two-photon photocurrent* and *voltage preservation*. Two-photon photocurrent is the production of extra sub-bandgap photocurrent from the absorption of two below bandgap photon energies. The voltage preservation implies that the voltage of an IBSC should only be limited to the fundamental semiconductor bandgap, and not to the sub-bandgaps. Voltage preservation only occurs if the quasi Fermi level (QFL) of the IB is separated/isolated from the QFLs of the VB and CB [6]. Demonstration of the two operating principles of the solar cells is a key step in the implementation of any high efficiency IBSC. These demonstrations can only be done at the device level, and in most cases sophisticated experimental procedures are required.

This paper is focused on the DL-IB materials, the least investigated IB materials so far. Si, II-VI, and III-V semiconductors heavily doped mainly by transition metals have been proposed as DL-IB materials [7–9]. The main DL-IB materials that have been investigated experimentally include: GaAs:Ti [6], Si doped by Ti [10], S [11], and Se [12]; GaN doped by Mn [13] and Cr [14]; $CuGaS_2$ doped by Fe [15] and Sn [16]; $CuInS_2$ doped by Ce [17] and Ti [18]; and $CuAlS_2$ doped by Ti [19]. None of these papers have reported the two-photon photocurrent; however, the voltage preservation has been demonstrated in GaAs:Ti at low temperatures [6].

Cr-doped ZnS (ZnS:Cr) is a potential DL-IB material and is the subject of this work. This material is particularly interesting as an IB material for three reasons: (i) An isolated partially filled IB was predicted in ZnS:Cr, with ~ 1.5 at% Cr [7]. (ii) An advantage with ZnS is that it is made of non-toxic and abundant elements, making ZnS:Cr an attractive solar cell material. (iii) ZnS:Cr has been a promising material for use as near- and mid-infrared lasers [20] and Cr has optically active energy levels in ZnS bandgap.

In contrast to the applications for IBSCs, a very low Cr content (typically below 4.0×10^{20} cm^3) is favorable for laser applications. However, a high sub-bandgap absorption, and consequently a high Cr

* Corresponding author.
E-mail address: nematollahim@gmail.com (M. Nematollahi).
URL: http://www.nematollahim.com (M. Nematollahi).

http://dx.doi.org/10.1016/j.solmat.2017.05.003
Received 15 November 2016; Received in revised form 30 April 2017; Accepted 3 May 2017
Available online 10 May 2017

content (1.5–5.0 at%) is required for use as an IB material compared to what is relevant for laser materials. A high doping density can also suppress the non-radiative recombination via multi-phonon emission [21].

In our previous work we observed that ZnS:Cr has very high sub-bandgap absorption coefficient compared to ZnS–with almost no sub-bandgap absorption [22]. In addition, the solar cells with ZnS:Cr (*n*-ZnO:Al/ZnS:Cr/p-Si) have shown much higher current density compared to the reference cells with ZnS [23]. This was attributed to the increased absorption, and partially to improvement in conductivity. In this work, we report a similar solar cell structure in which the p-type silicon is replaced by p-type gallium phosphide (GaP) with a wider bandgap, and here we refer to it as ZnS:Cr–IBSC. Specifically, we examine the two operating principles of the IBSCs in the ZnS:Cr–IBSC.

We present the quantum efficiency of the ZnS:Cr–IBSC measured at various temperatures in Section 3.1, and the voltage preservation study in Section 3.2. Based on these results, we propose an energy band diagram for ZnS:Cr in Section 3.3. A corresponding equivalent circuit model is given in Section 3.4, which is consistent with the suggested energy band diagram and can fully describe the characteristics of the ZnS:Cr–IBSC. In Section 3.5 we present the photocurrent produced by the ZnS:Cr–IBSC in the presence and absence of an additional light bias. Although there is no obvious evidence of the two photon photocurrent in the ZnS:Cr–IBSC, we observe an interesting two photon effect in the photocurrent. Finally, in Section 3.6 we discuss the contribution of the GaP substrate in photo-current and we show that the overall conclusions of this study are not affected if light is partially absorbed in GaP. The outcomes of this work are interesting and have never been measured in a solar cell based on ZnS, and we present an interpretation in the framework of IBSCs.

2. Experiments

2.1. Solar cell fabrication

The simplified structure of the ZnS:Cr–IBSC is shown in Fig. 1(a). Ideally, a p-type ZnS should be used as the p-emitter, but since p-ZnS is not available, we used p-GaP (Zn-doped) as an alternative substrate. The band diagram of the ZnS:Cr–IBSC is also given in Fig. 1(b). As can be seen, the band alignment of the solar cell is not ideal. Prior to the growth, the GaP substrate was etched by Hydrofluoric acid (5% solution) in order to remove the native oxides. A ZnS:Cr (≈1.3 at% Cr, thickness ≈1.97 μm) was grown on the GaP substrate at 200 °C by molecular beam epitaxy. We used the same procedure as in Ref. [22]. Then, in a separate chamber, a ZnO:Al layer (50 ± 5 nm) was deposited by pulsed laser deposition (KrF excimer laser Lambda Physics COMPex Pro 110, 248 nm) using a polycrystalline Al-doped ZnO target with 5 wt % Al. For simplicity, no back-surface passivation, or anti-reflection coating on the front surface was added. The Au/Al front contact was grown by sputtering with ≈100 nm thickness of each layer. Finally, a Pd/Zn/Pd back contact (≈200 nm) was grown and annealed at 250 °C for 7 min to form an ohmic contact with the p-GaP, having a resistance of 0.9 Ωcm^2.

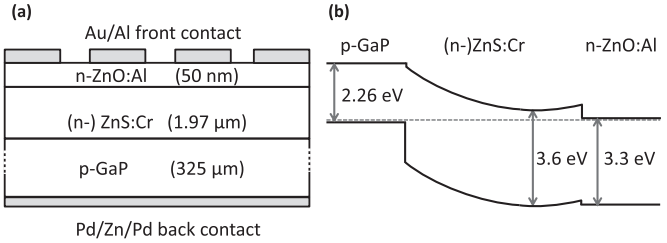

Fig. 1. (a) Schematic diagram of the ZnS:Cr–IBSC structure(ZnO:Al/ZnS:Cr/p-GaP), and (b) the band diagram of the ZnS:Cr–IBSC in equilibrium in dark condition; for simplicity the energy levels in the ZnS:Cr bandgap are not depicted (the x axis is out of scale).

2.2. Characterization methods

The external quantum efficiency (EQE) of the ZnS:Cr–IBSC was measured at room temperature using a halogen lamp and a NewPort Cornerstone 7400 monochromator equipped with appropriate second order optical filters, and calibrated Newport photodetectors. Afterwards, the sample was mounted in a vacuum chamber and cooled using a closed cycle He-gas cryostat. The EQE for temperatures below 297 K was calculated using the sample to calibrate the spectrum inside the cryostat. The output photocurrent (I_{ph}) was acquired with a lock-in amplifier synchronized to the frequency of a chopper (23 Hz) in front of the lamp. In a second experiment, the sample was illuminated with an additional continuous 0.65 μm (1.9 eV) light bias (AlGaInP laser diode). To study the voltage preservation, the V_{oc} was measured with concentrated light at various temperatures, following the details of the experimental condition found in Ref. [24].

3. Results and discussion

3.1. External quantum efficiency

Fig. 2 shows the EQE of the ZnS:Cr–IBSC at different temperatures. The first noticeable characteristic of the cell is that no response above the ZnS:Cr bandgap was detected. The room temperature ZnS:Cr bandgap, determined by spectroscopic ellipsometry, is in the range 3.5–3.6 eV, which is slightly lower than that of ZnS [22]. Note that the intensity of our monochromatic source is very low for $E \geq 3.6$ eV, which results in a higher noise level in EQE. As a result, the photocurrent and consequently the EQE above 3.6 eV is at the noise level of the measurement.

Next, it is important to note that the cell response is solely related to the ZnS:Cr for $E < 2.26$ eV, whereas for $E \geq 2.26$ eV the measured photocurrent can be partially related to the absorption in the GaP. We attribute the nearly abrupt increase in the EQE at ~ 2.3 eV to absorption and carrier generation in the GaP substrate for three reasons: (i) the transition matches well with the indirect bandgap of GaP at 2.26 eV; (ii) considering the thickness and the measured absorption coefficient of the ZnS:Cr film [25], nearly upto 45% of the photons with $E \geq 2.26$ eV can be absorbed in GaP; and (iii) with decreasing temperature, this abrupt increase is observed at a higher photon energy that fits well with the increase of the GaP bandgap with temperature reduction [26].

At room temperature, the EQE noticeably increases at $E_2 = 2.68$ eV

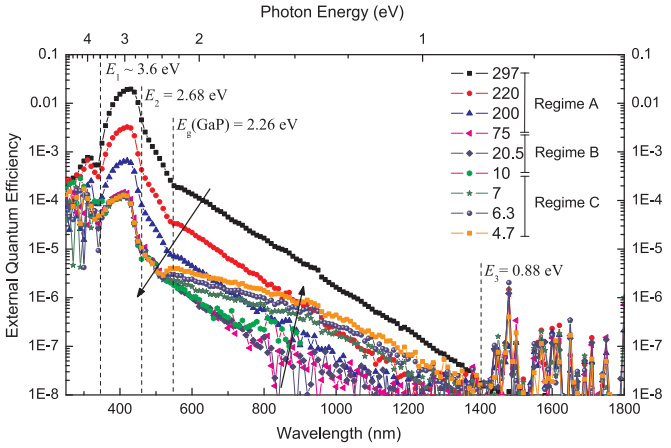

Fig. 2. External quantum efficiency (EQE) of the ZnS:Cr–IBSC at various temperatures. The vertical dashed lines show the GaP bandgap, the ZnS:Cr bandgap, E_1, and the two main transitions related to ZnS:Cr, E_2 and E_3. The two arrows indicate the change of the spectra with decreasing temperature. In regime A, the EQE decreases for all photon energies; in regime B, the EQE is almost constant for all photon energies; in regime C, the EQE increases for sub-bandgap photons.

and $E_3 = 0.88$ eV. We attribute both energies to electronic transitions in ZnS:Cr. The p-GaP substrate had no absorption below its indirect energy gap (not shown). Therefore, the absorption threshold at $E_3 = 0.88$ eV reveals the energy gap between the highest energy levels with electrons and the lowest energy level with holes in the ZnS:Cr. Consequently, this gives us an approximation of the position of the IB with respect to one of the energy bands, either the CB or the VB. Note that E_3 is measured close to the detection limit of the characterization system, and at low temperatures, it has a shift to higher energies. This is due to the relatively lower signal to noise ratio for the photocurrent measurements performed for $T \leq 220$ K.

As mentioned above, the measured photocurrent for $E \geq 2.26$ eV can be partially related to the absorption in the GaP. Specifically, E_2 is in proximity of the direct bandgap of GaP, that is, 2.8 eV. However, for two reasons we believe that E_2 can be related to electronic transitions in the ZnS:Cr layer. First, we found out that only up to 20% of light at this energy can enter GaP. Therefore, it is less likely that E_2 is due to the absorption in GaP. This was estimated from the absorption coefficient of a ZnS:Cr film grown under the same condition (not shown, see Ref. [25]). Second, the optical constants of ZnS:Cr are determined using a harmonic oscillator dispersion model in Ref. [25], and a Lorenz oscillator was used to account for the Cr related states within the ZnS:Cr bandgap. The center energy of the Lorenz oscillators were ~2.7 eV, which is approximately at the energy of the absorption threshold observed at E_2. Nevertheless, the overall discussion of this paper is not affected if one assumes that $E_2 = 2.68$ eV is partly related to carrier generation in GaP. This will be discussed in more detail.

Three regimes can be recognized in the changes of the EQE of the ZnS:Cr–IBSC when the temperature decreases (see Fig. 2):

Regime A, 297 − 75 K: I_{ph} (proportional to EQE) decreases for all photon energies.
Regime B, 75 − 10 K: I_{ph} is constant for all photon energies.
Regime C, 10 − 4.3 K: I_{ph} increases for $E \leq 2.3$ eV.

3.2. Voltage preservation study

To investigate the voltage preservation, we have measured V_{oc} versus temperature under concentrated light and the result is shown in Fig. 3. Recall that the IB material is isolated from the contacts by the emitters (See Fig. 1(b)); therefore, we expect the voltage to be limited by the GaP bandgap. However, at room temperature and under 1 Sun illumination, a very low V_{oc} of 94 mV was measured. The low V_{oc} can be due to a high level of non-radiative recombination. A high concentration of Cr in ZnS can result in a film with crystal defects and small grain size [22]. Such recombination processes can be suppressed when the solar cell is operated at lower temperatures. In addition, a small

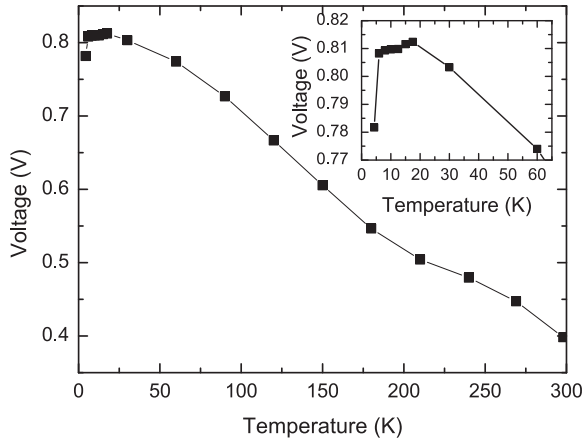

Fig. 3. Open-circuit voltage versus temperature under concentrated light for the ZnS:Cr–IBSC.

percentage of the Cr atoms can be optically inactive. This observation indicates that the fabricated solar cell is not suitable as a high efficiency IBSC under the current conditions, and that major improvements are required. The V_{oc} increased largely by the concentrated illumination, i.e., 4.3 times higher compared to the V_{oc} measured under 1 Sun illumination. The temperature reduction also increased the V_{oc}. However, as it can be seen in Fig. 3, the V_{oc} nearly saturates for $T \leq 20$ K to $V_{oc} \simeq 0.82$ V. It is interesting to note that the V_{oc} never surpasses the voltage associated to the lowest transition energy, i.e., E_3. In other words, the voltage is not recovered in the ZnS:Cr–IBSC, which means that a high level of thermal carrier escape from the IB is present in the ZnS:Cr–IBSC. More importantly, the thermalization process is not eliminated even at 4.3 K.

3.3. ZnS:Cr energy band diagram

Fig. 4(a) shows a schematic energy band diagram of ZnS:Cr, which we use to explain the behavior of the ZnS:Cr–IBSC. As mentioned above, the absorption threshold at $E_3 = 0.88$ eV indicates an approximation of the position of the IB with respect to one of the energy bands, either the CB or the VB. The as-grown ZnS:Cr has shown n-type behavior in the p-Si/ZnS:Cr heterojunctions [28]; thus, we can assume that the Fermi level is close to the conduction band minimum (CBM) under thermal equilibrium condition. Therefore, we can conclude that one IB in ZnS:Cr should be located near the CBM. This IB is labelled as IB_I, and it is illustrated with a dashed line in Fig. 4(a). Furthermore, the second absorption threshold observed in the EQE result indicates the position of a second IB, which is labelled as IB_{II} in Fig. 4(a). Note that the two IB levels have a finite energy width, but they are simply represented with two narrow dashed lines in Fig. 4(a).

Moreover, the low value of V_{oc} obtained at low temperature can be explained by the presence of a quasi-continuum of energy levels between the VBM and the IB_I energy level. The quasi-continuum of energy levels are depicted in Fig. 4(a). This energy level distribution would also explain why we can produce sub-bandgap photocurrent using “single” photon energies as low as 0.88 eV (that is, only with the monochromatic light). Indeed, a quasi-continuum of energy levels would allow a strong thermal generation to close the electrical circuit for the photo-current measurements. Note that the production of sub-bandgap photocurrent by two optical transitions through the IB has been demonstrated in IBSCs [4]. However, in the ZnS:Cr–IBSC studied here, due to thermal generation the measurement of sub-bandgap photo-current (and EQE) using “single” photon energies became possible.

Additionally, the presence of the quasi-continuum of energy levels in the band diagram of ZnS:Cr is in line with the previous study performed by resonant photoelectron spectroscopy technique reported in Ref. [27]. In that work, the Cr related energy levels have been directly measured, and a continuum of states above the VBM has been reported for ZnS:Cr made by the same growth method.

3.4. Equivalent circuit model

The electronic behavior of the ZnS:Cr–IBSC can be explained with the equivalent circuit–shown in Fig. 4(b)–in short circuit, which is the bias mode of the cell for EQE measurement. The circuit is based on the possible generation and recombination mechanisms illustrated in Fig. 4(a), but the generation and recombination in the GaP are not included in the model. I_{ph} is the current we measure, while the three current sources of I_1, I_2, and I_3 are associated with the three optical generations of g_1, g_2, and g_3, respectively. g_1, g_2, and g_3 correspond to the transitions VB–CB, IB_{II}–CB, and IB_I–CB, respectively (see Fig. 4(a)). In addition, the three diodes D_1, D_2, and D_3 are included to consider the recombination processes, regardless of the nature of these processes. We consider a series resistance R_s in the circuit. However, it is important to note that since I_{ph} is very low we neglect the effect of

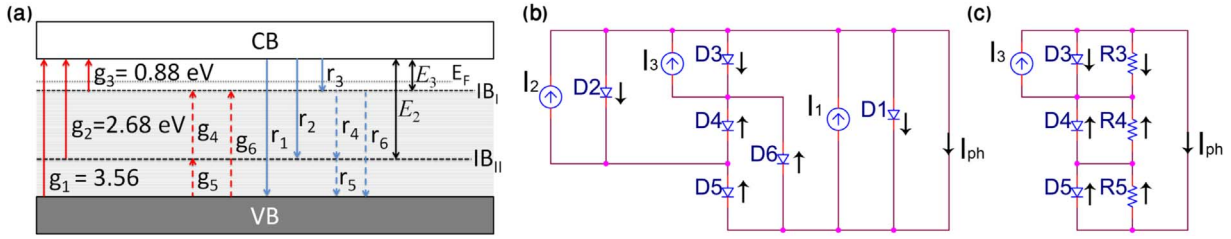

Fig. 4. (a) Schematic of the ZnS:Cr band diagram and the Cr energy levels based on this work and Ref. [27], (b) the ZnS:Cr–IBSC equivalent circuit in short-circuit condition, and (c) the simplified equivalent circuit for $E \leq 2.26$ eV. For simplicity the parallel resistances are not depicted in (b).

the series resistance in the rest of the discussion. To close the circuit, we need to include g_4, g_5, and g_6. These generations are assumed to be thermal generations, and are illustrated in Fig. 4(a). Accordingly, they are inherently included in the three diodes D_4, D_5, and D_6 by means of the diode term "-1" of its current-voltage characteristic. Because we have a quasi-continuum of energy levels between the VBM and the IB_I energy level, one can also assume that the three diodes of D_4, D_5, and D_6 are an approximation for many diodes in series connection, representing the recombinations. Also note that no shunt resistances are depicted in Fig. 4(b), for simplicity.

The current flowing through each diode D_i is $I_{D_i} = I_{0_i}(exp(qV_{D_i}/mkT) - 1)$ for $i = 1 - 6$, where V_{D_i} is the diode bias voltage associated to the quasi-Fermi level split between the bands involved, m is the diode ideality factor, and I_{0_i} is the diode saturation current. Considering the equivalent small signal resistance of $r_i = dV_{D_i}/dI_{D_i} = (mkT/q)(I_{D_i} + I_{0_i})^{-1}$ for the diodes, D_4 and D_5 would have the lowest resistances compared to the other diodes. As a result, D_2 and D_3 are biased nearly at the same voltage. This voltage cannot exceed the lower voltage that is related to D_3. Therefore, V_{oc} of the ZnS:Cr–IBSC is limited to the lowest energy gap. Similarly, V_{oc} is also limited to the lowest energy gap for high energy photons that can pump electrons from the VB to the CB.

To avoid the complexities, we restrict the discussion to the case where $E \leq 2.26$ eV. The corresponding equivalent circuit for this case is shown in Fig. 4(c). In this situation, the only current source would be I_3. Also note that the effects of the r_1, r_2, and r_6 recombinations are negligible compared to the other three recombinations, i.e., r_3, r_4, and r_5. Thus, only D_3, D_4, and D_5 are kept. In addition, for each diode a parallel resistance is considered, namely, R_3, R_4 and R_5. These resistances represent alternative paths for electron transitions that do not depend on the temperature and do not follow the temperature dependence established by the Shockley equation, such as a tunnel escape mechanism [29].

Therefore, for $E \leq 2.26$ eV, the three regimes of the EQE variation with temperature can be explained based on the circuit presented in Fig. 4(c):

Regime A, $297 - 75$ K: A constant current of I_3 is produced via IB_I-CB transition. Assuming that the equivalent resistances for D_4 and D_5 are low, this generated current does not go through the parallel resistances R_4 and R_5. Instead, it goes through the two diodes. When the temperature decreases to 75 K, the diode saturation currents of D_4 and D_5 decrease; consequently, the corresponding equivalent resistances of those diodes increase. Hence, I_{ph} decreases with decreasing temperature. From the temperature dependence of the EQE, we obtained the carrier escape activation energy [30]. The activation energy in regime A was determined to be nearly 200 meV. This indicates that the distribution of the quasi-continuum of energy levels can have a gap of 200 meV.

Regime B, $75 - 10$ K: Again, a constant current of I_3 is produced via IB_I-CB transition. But the temperature is low enough so that the current does not flow through D_4 and D_5 any more. Instead, it goes through the parallel resistances, R_4 and R_5. As these resistances do not vary when the temperature is further reduced, a constant I_{ph} is observed.

Regime C, $10 - 4.3$ K: In this case, the generated current I_3 still goes through the parallel resistances R_4 and R_5. However, the temperature is very low and the population of the E_3 energy level is expected to increase when the temperature decreases. The lower the temperature the higher the occupancy of such states; thus I_3 increases with decreasing temperature. As is seen in Fig. 3, the V_{oc} slightly decreases for $T \leq 10$ K, i.e., in regime C. Then, at 4.3 K, V_{oc} is about 0.78 V. This can indicate that the population of the levels below IB_I are enhanced and consequently the energy gap between the IB_I and the CB is reduced (see Fig. 3 for 4.3 K).

3.5. Photo-current under light bias

In a second experiment, we measured the photocurrent produced in the ZnS:Cr–IBSC in the presence and absence of an additional light bias at 4.3 K. As can be seen in Fig. 5, the photocurrent is decreased largely when the light bias is used. Note that the energy of the light bias is ~1.9 eV; hence we can cause the IB_I–CB transitions, but not the IB_{II}–CB one. The simplified equivalent circuit of the ZnS:Cr–IBSC shown in Fig. 4(c) can be used to explain the change in the photocurrent after this light bias was used. Note that the light bias is a constant DC light compared to the chopped monochromatic light. In the presence of the light bias, I_{D3} increases, which results in the reduction of the equivalent resistance for D_3. As a result, the generated current can recombine more in D_3 compared to the measurement with no bias. Hence a lower photocurrent is measured. In Fig. 5, the photocurrent is also slightly decreased for $E \simeq 3$ eV. In this case, most of the current can return through R_5. Therefore, the current generated via IB_{II}–CB transition is partially reduced by recombination in D_3.

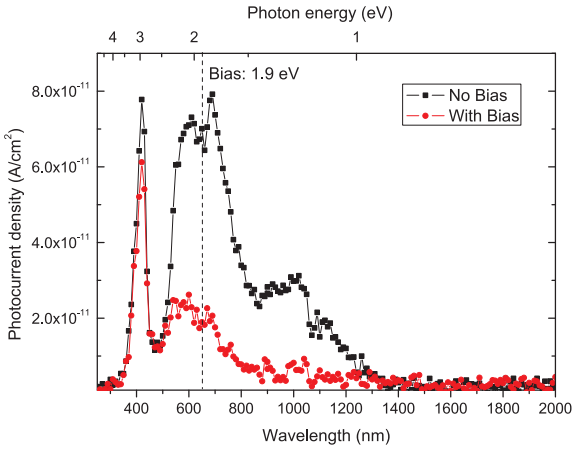

Fig. 5. Spectral photocurrent of the ZnS: Cr–IBSC at 4.3 K (square), and when the 1.9 eV laser bias is applied (circle). The spectral correction for the lamp intensity is not performed.

3.6. Photo-current generated by GaP

We now consider the case that the $E_2 = 2.68$ eV absorption threshold observed in the EQE result can be partly caused by light absorption in the GaP substrate (see Fig. 2). As mentioned earlier, the measurements of the absorption coefficient of the ZnS:Cr film have shown that more than 80% of the light at $E \sim 2.7$ eV is absorbed in the ZnS:Cr layer. In other words, only up to 20% of the light can reach to the GaP substrate. This result was achieved for a ZnS:Cr film with the same Cr content and thickness ($\approx$1.3 at% Cr $\approx$1.97 μm) grown on a Si substrate simultaneously.

Now, even if we assume that all the absorbed light in both ZnS:Cr and Gap results in charge carrier generation, the non-radiative recombination lifetime of the two materials might be very different. As a result, the GaP can have a higher share in the observed photo-current at $\sim$ 2.7 eV compared to that of ZnS:Cr. In this case, the only conclusion that cannot be supported would be the position of the IB_{II} in ZnS:Cr. It is important to note that the position of the IB_I at 0.88 eV below the CBM, and the presence of quasi-continuum of energy levels do not rely on the presence of IB_{II}. Therefore, we emphasize that the overall conclusion of this study is not affected if the absorption threshold at $E_2 = 2.68$ eV is partly related to carrier generation in GaP.

4. Conclusions

In summary, ZnS:Cr–IBSC (*n*-ZnO:Al/ZnS:Cr/p-GaP) was fabricated to study the ZnS:Cr as a potential intermediate band material. With this cell structure, the ZnS:Cr (and the IB) is electrically isolated from the contacts; thus, we expect the V_{oc} to be limited only by the lowest energy gap, the GaP bandgap. However, we observed a low V_{oc} of $\simeq$0.8 V at 4.3 K under concentrated light. In addition, the ZnS:Cr–IBSC was capable of producing photo-current when illuminated solely with "single" sub-bandgap photon energy of $E \geq 0.88$ eV.

Based on these observations and in line with the previous studies on ZnS:Cr, it was concluded that the ZnS:Cr made for this work exhibits a quasi-continuum of energy levels above its valence band maximum. We also concluded that the lowest energy gap in ZnS:Cr is nearly 0.8 eV. Specifically, we discussed that ZnS:Cr has two energy levels at 0.88 eV (IB_I) and 2.68 eV (IB_{II}) below the conduction band minimum. Consequently, the quasi-continuum of energy levels caused thermal carrier generation, and restricted the V_{oc} to the lowest transition, i.e., IB_I–CB. Therefore, the Cr energy levels in the bandgap of highly doped ZnS:Cr are determined. This information can be used to evaluate the theoretical efficiency limit of the ZnS:Cr–IBSCs, but this is not the concern of this paper. It is also important to note that as long as the quasi-continuum of energy levels are present in the bandgap, one cannot expect a high open-circuit voltage and short-circuit current in such ZnS:Cr–IBSC. Doping ZnS with a high Cr concentration results in a film with small grain structure, impurities and crystal defects, which lead to the formation of the quasi-continuum of localized energy levels in the bandgap. This reveals a technological challenge in fabrication of DL-IB materials with a high density of deep-levels. The future work on ZnS:Cr should focus on the improvement of the ZnS:Cr crystal quality, to shrink the width of the intermediate bands and to lower the thermal carrier escape.

Acknowledgments

This work is done in part within the Norwegian Center for Solar Cell Technology (project number 193829). The authors also acknowledge the research council of Norway for financial support via the Nano2021 program (project number 203503). IES-UPM also acknowledge the financial support of the Comunidad de Madrid through the project MADRID-PV (grant number S2013/MAE-2780). We thank Prof. Ursula Gibson for comments that greatly improved the manuscript, and Thomas Brakstad for assistance with Spectroscopic Ellipsometry measurement.

References

[1] A. Luque, A. Marti, Increasing the efficiency of ideal solar cells by photon induced transitions at intermediate levels, Phys. Rev. Lett. 78 (26) (1997) 5014.
[2] A. Luque, A. Marti, C. Stanley, Understanding intermediate-band solar cells, Nat. Photonics 6 (3) (2012) 146–152.
[3] I. Ramiro, A. Marti, E. Antolin, A. Luque, Review of experimental results related to the operation of intermediate band solar cells, IEEE J. Photovolt. 4 (2) (2014) 736–748.
[4] E. López, A. Datas, I. Ramiro, P.G. Linares, E. Antolín, I. Artacho, A. Martí, A. Luque, Y. Shoji, T. Sogabe, A. Ogura, Y. Okada, Demonstration of the operation principles of intermediate band solar cells at room temperature, Sol. Energ. Mat. Sol. C 149 (2016) 15–18.
[5] T. Tanaka, M. Miyabara, Y. Nagao, K. Saito, Q. Guo, M. Nishio, K.M. Yu, W. Walukiewicz, Photogenerated current by two-step photon excitation in ZnTeO intermediate band solar cells with n-ZnO window layer, IEEE J. Photovolt. 4 (1) (2014) 196–201.
[6] P.G. Linares, A. Martí, E. Antolín, I. Ramiro, E. López, E. Hernández, D. Fuertes Marrón, I. Artacho, I. Tobías, P. Gérard, C. Chaix, R.P. Campion, C.T. Foxon, C.R. Stanley, S.I. Molina, A. Luque, Extreme voltage recovery in GaAs:Ti intermediate band solar cells, Sol. Energ. Mat. Sol. C 108 (2013) 175–179.
[7] C. Tablero, Optoelectronic properties of Cr-substituted II-VI semiconductors, Comp. Mater. Sci. 37 (4) (2006) 483–490.
[8] C. Tablero, Survey of intermediate band material candidates, Solid State Commun. 133 (2) (2005) 97–101.
[9] K. Sanchez, I. Aguilera, P. Palacios, P. Wahnón, Formation of a reliable intermediate band in Si heavily coimplanted with chalcogens (S, Se, Te) and group III elements (B, Al), Phys. Rev. B 82 (2010) 165201.
[10] H. Castán, E. Pérez, H. García, S. Dueñas, L. Bailón, J. Olea, D. Pastor, E. García-Hemme, M. Irigoyen, G. González-Díaz, Experimental verification of intermediate band formation on titanium-implanted silicon, J. Appl. Phys. 113 (2) (2013) 24104.
[11] M.T. Winkler, D. Recht, M.-J. Sher, A.J. Said, E. Mazur, M.J. Aziz, Insulator-to-metal transition in sulfur-doped silicon, Phys. Rev. Lett. 106 (2011) 178701.
[12] S. Zhou, F. Liu, S. Prucnal, K. Gao, M. Khalid, C. Baehtz, M. Posselt, W. Skorupa, M. Helm, Hyperdoping silicon with selenium: solid vs. liquid phase epitaxy, Sci. Rep. 5 (2015) 8329.
[13] J.-K. Sheu, F.-W. Huang, Y.-H. Liu, P.C. Chen, Y.-H. Yeh, M.-L. Lee, W.-C. Lai, Photoresponses of manganese-doped gallium nitride grown by metalorganic vapor-phase epitaxy, Appl. Phys. Lett. 102 (7) (2013) 071107.
[14] S. Sonoda, Partially filled intermediate band of Cr-doped GaN films, Appl. Phys. Lett. 100 (20) (2012) 202101.
[15] B. Marsen, S. Klemz, T. Unold, H.-W. Schock, Investigation of the sub-bandgap photoresponse in $CuGaS_2$:Fe for intermediate band solar cells, Prog. Photovolt. Res. Appl. 20 (6) (2012) 625–629.
[16] C. Yang, M. Qin, Y. Wang, D. Wan, F. Huang, J. Lin, Observation of an intermediate band in Sn-doped chalcopyrites with wide-spectrum solar response, Sci. Rep. 3 (2013) 1286.
[17] L. Xiao, J. Zhu, T. Ding, Y. Wang, Y. Fan, Q. Bo, Synthesis and characterization of Ce-incorporated $CuInS_2$ chalcopyrites, Mater. Lett. 159 (2015) 392–394.
[18] B. Marsen, L. Steinkopf, A. Singh, H. Wilhelm, I. Lauermann, T. Unold, R. Scheer, H.-W. Schock, Effects of Ti-incorporation in $CuInS_2$ solar cells, Sol. Energ. Mat. Sol. C 94 (10) (2010) 1730–1733.
[19] C. Guo, C. Yang, Y. Xie, P. Chen, M. Qin, R. Huang, F. Huang, Preparation of Sn-doped $CuAlS_2$ films with an intermediate band and wide-spectrum solar response, RSC Adv. 6 (47) (2016) 40806–40810.
[20] N.A. Vlasenko, P.F. Oleksenko, M.A. Mukhlyo, Z.L. Denisova, L.I. Veligura, ZnS:Cr and ZnSe:Cr thin-film waveguide structures as electrically pumped laser media with an impact excitation mechanism, Ann. Phys. 525 (12) (2013) 889–905.
[21] A. Luque, A. Martí, E. Antolín, C. Tablero, Intermediate bands versus levels in non-radiative recombination, Phys. B Condens Matter 382 (1–2) (2006) 320–327.
[22] M. Nematollahi, X. Yang, Aas, Lars Martin Sandvik, Z. Ghadyani, M. Kildemo, U.J. Gibson, T.W. Reenaas, Molecular beam and pulsed laser deposition of ZnS:Cr for intermediate band solar cells, Sol. Energ. Mat. Sol. C. 141 (2015) 322–330.
[23] M. Nematollahi, Cr-doped ZnS for intermediate band solar cells, (Ph.D. thesis), Department of Physics, NTNU (2014).
[24] P.G. Linares, A. Martí, E. Antolín, I. Ramiro, E. López, C.D. Farmer, C.R. Stanley, A. Luque, Low-temperature concentrated light characterization applied to intermediate band solar cells, IEEE J. Photovolt. 3 (2) (2013) 753–761.
[25] T. Brakstad, B. R. Hope, M. Nematollahi, M. Kildemo, N. J. Podraza, K. Ghimire, T. W. Reenaas, Ellipsometric study of the optical sesponse of ZnS:Cr for PV applications, Article in press:Appl. Surf. Sci.
[26] M.R. Lorenz, G.D. Pettit, R.C. Taylor, Band gap of gallium phosphide from 0 to 900K and light emission from diodes at high temperatures, Phys. Rev. 171 (3) (1968) 876.
[27] F. Mazzola, M. Nematollahi, Z.S. Li, S. Cooil, X. Yang, T.W. Reenaas, J.W. Wells, Resonant photoemission spectroscopy for intermediate band materials, Appl. Phys. Lett. 107 (19) (2015) 192104.
[28] X. Yang, M. Nematollahi, U.J. Gibson, T.W. Reenaas, Cr-doped ZnS for intermediate band solar cells, Photovoltaic Specialists Conference (PVSC), 2013 IEEE 39th.
[29] I. Ramiro, E. Antolín, A. Martí, C.D. Farmer, C.R. Stanley, A. Luque, Experimental demonstration of the effect of field damping layers in quantum-dot intermediate band solar cells, Sol. Energ. Mat. Sol. C 140 (2015) 299–305.
[30] E. Antolín, A. Martí, C.D. Farmer, P.G. Linares, E. Hernández, A.M. Sánchez, T. Ben, S.I. Molina, C.R. Stanley, A. Luque, Reducing carrier escape in the InAs/GaAs quantum dot intermediate band solar cell, J. Appl. Phys. 108 (6) (2010) 064513.